# scientific reports

OPEN

# Physico-chemical features and membranolytic activity of dust from low or no crystalline silica engineered stone with implications for toxicological assessment

Chandnee Ramkissoon[1,5]✉, Cristina Pavan[2,3,5]✉, Jasmine Rita Petriglieri[3,4], Marianna Fimiani[2,3], Dino Pisaniello[1], Sharyn Gaskin[1] & Francesco Turci[2,3]

The re-emergence of silicosis among engineered stone (ES) workers has prompted the development of low- to no-crystalline silica ($SiO_2$) ES products, marketed as safer alternatives to traditional high-$SiO_2$ ES. However, the composition of these new materials—often incorporating recycled minerals, binders, and pigments—remains complex and poorly characterized in terms of potential health risks. This study assessed the physico-chemical properties and membranolytic activity of dusts generated by mechanical processing of five ES samples (ranging from 90 to 0 wt% $SiO_2$) and a natural stone as comparison. Dusts were analyzed for particle size distribution, mineralogy, morphology and zeta potential. A standard membranolysis assay was used to assess relative cytotoxicity. Dusts from new ES slabs contained lower quartz and cristobalite levels (23 to 0 wt%) than traditional ES, with crystalline silica replaced predominantly by silicates, aluminosilicates, amorphous phases, or gibbsite. Untreated ES dusts showed little membranolytic activity. However, after heating to remove organic binding resins, a high membranolytic activity was observed for traditional ES, and to a lesser degree for low-$SiO_2$ ES. No activity was observed in no-$SiO_2$ ES, composed primarily of gibbsite. Our findings suggest that reducing crystalline silica content may mitigate certain toxicological risks. However, the diverse and evolving composition of alternative ES products warrants ongoing toxicological evaluation.

**Keywords** Engineered stone, Low silica, No silica, Silicosis, Physico-chemical, Membranolysis, Cytotoxicity

Engineered stone (ES) is an artificial stone material typically comprising 90 wt% crystalline silica ($SiO_2$), natural stone aggregates and pigments bound together with organic resins to form slabs of various colors and designs[1,2]. Its popularity for kitchen and bathroom benchtop applications is largely attributed to its aesthetic appeal, structural durability, and lower cost compared to natural stones such as marble and granite. However, its rise in popularity has brought about a re-emergence of occupational lung disease among workers, likely caused by exposure to high levels of respirable crystalline silica (RCS) during the processing of ES slabs[3–7]. In Australia, the first case of ES-associated silicosis emerged in 2015; by 2022, 579 cases had been identified[8]. According to the multinational Engineered Stone Silicosis Investigators (ESSI) Global Silicosis Registry[9] countries like Israel[7] Spain[10–12] Belgium[13] the USA[14] and more recently the UK[15] appear to follow a similar increasing trend in silicosis cases. In Italy, an high silicosis incidence rate in workers exposed to ES dust has been reported (24 cases of silicosis out of 45 workers recruited)[16].

In the light of the above, there has been a call for measures to better protect workers against exposure to RCS, thus reduce health risks in the ES industry. These measures included reducing or eliminating the $SiO_2$ content of ES slabs, as well as tightening of regulations for all processes that use $SiO_2$-containing materials. Australia has become the first country to ban $SiO_2$-containing ES (>1 wt%)[17,18] and other countries like the UK have called on their government to follow suit[19]. This represents a significant shift aligned with the highest

[1]School of Public Health, Adelaide Exposure Science and Health, The University of Adelaide, Adelaide, SA, Australia. [2]Department of Chemistry, University of Turin, Turin 10125, Italy. [3]"G. Scansetti" Interdepartmental Center for Studies on Asbestos and Other Toxic Particulates, University of Turin, Turin 10125, Italy. [4]Department of Earth Sciences, University of Turin, Turin 10125, Italy. [5]Chandnee Ramkissoon and Cristina Pavan contributed equally to this work. ✉email: chandnee.ramkissoon@adelaide.edu.au; cristina.pavan@unito.it

level of action – elimination, according to the hierarchy of hazard controls for occupational health and safety[20]. Consequently, manufacturers have introduced low- to no-$SiO_2$ ES benchtop products[21] which are marketed as safer alternatives to traditional ES. However, there is currently insufficient scientific evidence to support the assumption that these reformulated materials pose a lower health risk than their high-$SiO_2$ counterparts. In fact, recent research has shown that components of ES, other than $SiO_2$, e.g., metals and resins, are likely to play a role in the pathogenesis of ES-associated disease[22]. Furthermore, several new stone formulations, although low in crystalline $SiO_2$, contain various inorganic aggregates and fillers, including recycled glass, feldspar, and other minerals. These dust may still pose a risk to workers upon inhalation, particularly in the submicron size range. Finally, a recent study examining $SiO_2$ nanoparticles from ES product fabrication has emphasized that surface characteristics of nanoparticles are important, but these comprise about 1% of the aerosol mass, compared with 4–24% of the aerosol surface area[23]. Thus, trace or low levels of $SiO_2$ may still be important, and the current RCS metric, being based on mass may not provide adequate protection.

The aim of this study was to assess the physico-chemical properties and membranolytic activity (*via* the hemolysis assay) of dust generated by mechanically processing new-generation low- to no-$SiO_2$ ES to help understand their hazard potential. Membranolysis of the phagolysosome membrane is thought to be a key step in the development of lung inflammatory response and silicosis[24,25] and red blood cells (RBCs) are commonly used to test membranolytic effects of inhalable dust, particularly in occupational studies involving silica and metal oxide particles[26,27].

Five ES dust samples with varying $SiO_2$ content (from 0 to 90 wt%) were analyzed. In decreasing $SiO_2$ content, the samples were: High-$SiO_2$ ES1, Low-$SiO_2$ ES2, Low-$SiO_2$ ES3, No-$SiO_2$ ES4 and No-$SiO_2$ ES5. For comparison, one quartzite natural stone (NS) was also included[28]. Dust was generated by mechanical processing using two approaches. For samples ES1, ES2, ES3, and NF, dust was produced by simulating cutting with an angle grinder in a confined environment[28] replicating the most critical condition for worker exposure to ES dust. Due to limited sample availability, ES4 and ES5 were processed by ball milling. This method can replicate the high-energy particle generation typical of cutting operations, in terms of particle morphology, size, and surface reactivity[29]. To minimize variability, the milling protocol was optimized to produce a particle size distribution comparable to that of dust from actively-cut ES samples.

The outcomes of our research may help to establish and rank the risk associated with dust from these emerging low- to no-$SiO_2$ composite materials. Our study provides timely and novel data that are crucial for regulatory decision making.

## Results

### Physico-chemical characterization

*Particle size*

The diameters and particle size distribution curves of ES1-5 and NS dusts were measured by laser diffractometry and are reported in Table 1 and Fig. S1 (Supplementary Information), respectively. The mass median diameter (MMD) of particles, represented by $d(0.5)$ in Table 1, differed minimally across stone samples (range of 10.2 μm to 13.3 μm). Some differences were observed in the size distributions (Fig. S1) that could be attributed to slab composition or different processing methods. The bi-modal size distributions of No-$SiO_2$ ES4 and No-$SiO_2$ ES5, which were generated by milling, showed a small proportion of fine particles (Fig.S1 D-E), while actively cut samples tended to have multimodal distributions with larger particles, for example High-$SiO_2$ ES1, Low-$SiO_2$ ES2 and Low-$SiO_2$ ES3 (Fig.S1 A-C). However, Low-$SiO_2$ ES3 (Fig.S1 C) also exhibited a fine particle population, despite the dust being generated by cutting. This suggests that the material composition may also influence the resulting particle size distribution. Natural stone sample was the only stone sample with a monomodal size distribution, suggesting homogenous size fractionation when NS was processed, relative to ES.

Scanning Electron Microscopy (SEM) micrographs (Fig. 1A) further evidenced the broad range of particles sizes that characterized each dust sample, particularly ES samples, as expected for dust obtained by mechanical processing, either cutting or milling.

*Morphology and elemental composition*

The particle morphology of ES samples and NS is illustrated in Fig. 1A, where SEM secondary electron micrographs of selected particles are reported. The dust particles generated from $SiO_2$-containing stone

| Stone sample | d(0.1) μm | d(0.5) μm | d(0.9) μm |
|---|---|---|---|
| High-$SiO_2$ ES1[†] | 3.21 | 11.6 | 43.2 |
| Low-$SiO_2$ ES2[†] | 4.24 | 11.0 | 26.2 |
| Low-$SiO_2$ ES3[†] | 2.09 | 11.3 | 33.3 |
| No-$SiO_2$ ES4[§] | 0.239 | 10.2 | 24.6 |
| No-$SiO_2$ ES5[§] | 0.236 | 10.2 | 24.4 |
| NS[†] | 4.78 | 13.3 | 28.2 |

**Table 1**. Volume particle size distribution parameters for dust obtained by mechanical processing of engineered stones (ES1-5) and one natural stone (NS). Results $d(0.1)$, $d(0.5)$ and $d(0.9)$ indicate that 10%, 50% and 90% of the particles were smaller than or equal to the size reported[30]. [†]Generated by dry-cutting; [§]Generated by milling.
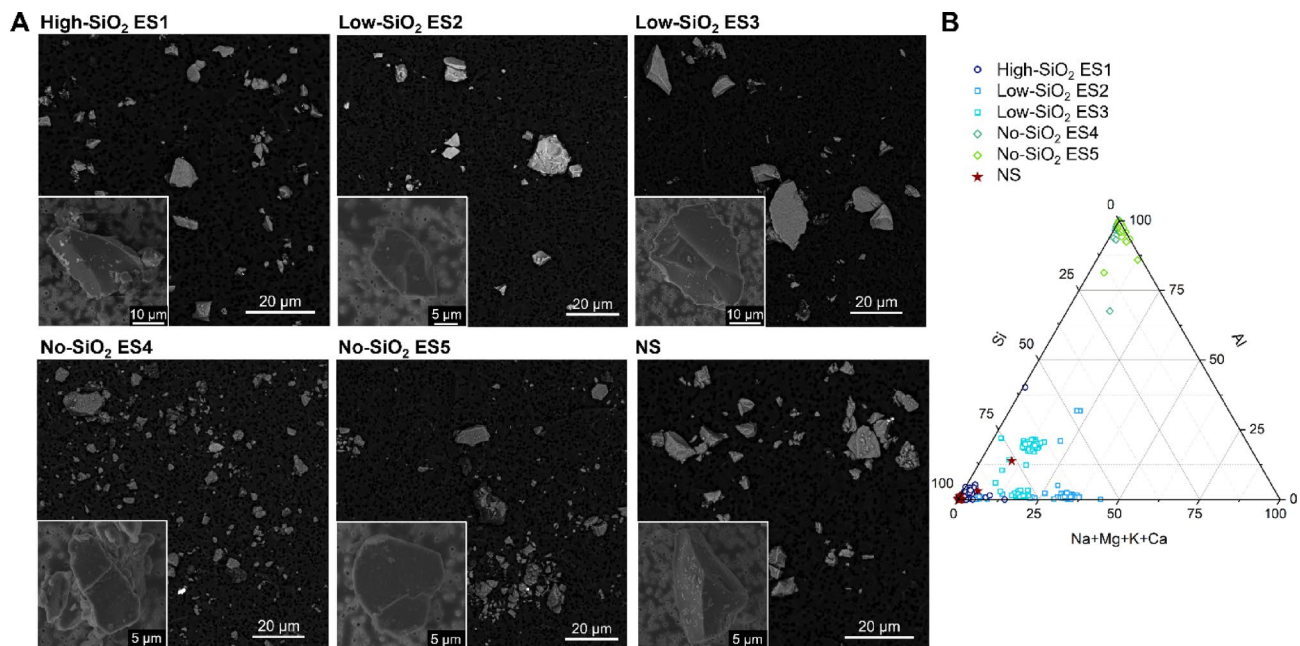
**Fig. 1**. **A** SEM micrographs showing size and morphology of engineered stone (ES1-5) and natural stone (NS) dusts. Representative micrographs were taken at low (5,000×, main images) and high (15,000× to 20,000×, inset images) magnifications. Different scale bars are reported in each image. **B** Ternary diagram of ES1-5 and NS dusts obtained by EDS. The ternary plot shows the variability in chemical composition (Si, Al, and Na + Mg + K + Ca) of the dusts, expressed in wt%. Each dot is associated with the EDS analysis of one single particle.

samples (ES1-3 and NS) exhibited surface conchoidal fractures, irregular shapes, and sharp edges, reflecting the morphology of quartz particles obtained by mechanical fracturing, including grinder processing and milling[28,31]. Larger particles showed smaller ones adhered to their surface, possibly by electrostatic forces[32]. In comparison, No-SiO$_2$ ES4 and 5 particles exhibited relatively smoother surfaces and rounder edges (Fig. 1A).

The ternary diagram (Fig. 1B) showed the variability in chemical composition of ES and NS dusts determined by Energy Dispersive X-ray Spectroscopy (EDS) analysis. Results were in line with the expected content of SiO$_2$ for each sample. The High-SiO$_2$ ES1 was mainly composed by Si particles (ca. 90–100 wt%). The Low-SiO$_2$ ES2 and ES3 had a more heterogeneous composition due to the presence of different alkaline and alkaline earth metals (Na + Mg + K + Ca), in addition to Si, signalling the presence of silicates. The No-SiO$_2$ ES3 and ES4 showed almost no Si content (with some exceptions) and a high content of Al. This suggests that minerals other than SiO$_2$ constituted the Low- and No-SiO$_2$ samples. The NS particles showed a virtually 100% SiO$_2$ composition, indicating that this sample, i.e., quartzite, consisted mostly of silica, with only a few particles containing metals due to contaminant minerals. Overall, the High-SiO$_2$ ES1 and NS samples, as well as the No-SiO$_2$ ES4 and ES5 samples exhibited relatively homogenous composition, primarily consisting of Si- and Al-rich particles, respectively. Conversely, the Low-SiO$_2$ ES2 and ES3 consisted of different mineral phases, suggesting that crystalline silica was accompanied by various silicates and aluminosilicates.

*Mineral phases*

The mineralogical composition of the ES dust samples was determined using a combination of quantitative X-Ray Diffraction (XRD) and qualitative micro-Raman spectroscopy. These two techniques offered complementary insights. XRD provided quantitative data on crystalline mineral phases but did not detect amorphous components. In contrast, Raman spectroscopy identified both amorphous and organic (non-crystalline) phases, although being only semi-quantitative. Mineral composition of each dusts differed significantly depending on the formulation of the originating slab (Table 2; Fig. 2). In particular, the crystalline SiO$_2$ content of ES dusts was well correlated with the crystalline SiO$_2$ content in the slab, reported in manufacturer's safety data sheets (SDS). High-SiO$_2$ ES1 generated a high level (> 75%) of crystalline SiO$_2$ during cutting, with twice as much quartz as cristobalite. Qualitative assessment by Raman spectroscopy identified also titanium dioxide (rutile). Low-SiO$_2$ ES2 and ES3 dusts contained < 25% and < 10% crystalline SiO$_2$, respectively. Other phases in low-SiO$_2$ ES dusts were silicates, including amorphous vitreous phase (VP) particles, feldspar (i.e., albite, NaAlSi$_3$O$_8$) and mica (i.e., muscovite, KAl$_2$Si$_3$AlO$_{10}$(OH)$_2$). Titanium dioxide (rutile) was also detected. The crystalline SiO$_2$ content of No-SiO$_2$ ES4 and ES5 particles was below the analytical limit of detection (LOD, approximately 1 wt% for XRPD), providing evidence in support to the manufacturers' "zero-silica" claim. ES4 and ES5 dust was almost entirely composed of aluminium hydroxide mineral (i.e. gibbsite, Al(OH)$_3$). In line with the EDS results (Fig. 1B), the dust generated from NS quartzite showed a high level of crystalline SiO$_2$ (> 80%), in the form of quartz only. The

| Stone sample | Mineral phases (%) | | Specific surface area (m²/g) | Weight loss after heating (%) |
|---|---|---|---|---|
| | Crystalline silica (quartz + cristobalite) | Other phases* | | |
| High-SiO₂ ES1 | 76 (53 + 23) | Rutile, GC | 1.16 | 10.8 |
| Low-SiO₂ ES2 | 23 (23 + n.d.) | VP, GC, rutile | 1.52 | 12.4 |
| Low-SiO₂ ES3 | 7.0 (4.5 + 2.5) | Albite, rutile, GC, VP, muscovite | 0.79 | 12.1 |
| No-SiO₂ ES4 | 0.0 (n.d. + n.d.) | Gibbsite, GC | 6.02 | 46.0 |
| No-SiO₂ ES5 | 0.0 (n.d. + n.d.) | Gibbsite, GC | 6.56 | 46.0 |
| NS | 81 (81 + n.d.) | VP, GC | 2.60 | Not applicable† |

**Table 2**. Physico-chemical characteristics of engineered stone (ES1-5) and natural stone (NS) dusts. The crystalline silica content was measured by quantitative XRD. The other phases were qualitatively assessed by Raman spectroscopy. The specific surface area was measured by the BET method and weight loss after heating was measured by TGA. *In decreasing order of quantity;. 'n.d.', not detected (below analytical limits);. 'GC': glassy carbon; 'VP': vitreous phase;. †Not applicable to natural stone, which does not contain resin.



**Fig. 2**. Doughnut charts of engineered stone (ES1-5) and natural stone (NS) dusts illustrating mineral phases and resin content measured by Raman spectroscopy. Each chart displays the relative content of mineral phase that is coated with resin (decorated pattern). Abbreviations were based on Whitney and Evans (2010)[34]: Qtz: quartz; Crs: cristobalite; Rt: rutile; GC: glassy carbon; Ab: albite; Ms: muscovite; Gbs: gibbsite; VP: vitreous phase.

rest of the NS composition was amorphous, with two minor equal contributions from inorganic vitreous phase (VP) and glassy carbon (GC)[33].

*Specific surface area*
The specific surface area (SSA) of ES1-ES3 ranged from 0.79 to 1.52 m²/g, while ES4 and ES5 showed a higher SSA of 6.02 and 6.06 m²/g, respectively (Table 2). Besides the different mineralogy of the samples, this difference could be due to the dust generation methods used – milling *vs.* grinder processing, as discussed above. The NS dust particles exhibited a SSA of 2.60 m²/g.

*Organic content and characterization*
High to Low-SiO₂ ES samples contained 11–12 wt% organic resin, measured by thermogravimetric analysis (TGA) (Table 2). No-SiO₂ ES samples lost 46% weight after pyrolysis, likely due to a combination of resin

decomposition and dehydration of gibbsite (Al(OH)$_3$) as it converts to alumina (Al$_2$O$_3$), estimated to be 35 wt% at 600°C[35]. The Raman spectra relative to the resin in ES dusts (Supplementary Information, Fig. S2) were recorded on isolated particles that did not include inorganic minerals, except for ES4 and ES5. All Raman spectra were very similar and were assigned to a polystyrene and polymethyl methacrylate (PS-PMMA) co-polymer[36]. In ES4 and ES5 we were unable to detect particles of pure organic resin, as evidenced by the superimposed Raman spectra of gibbsite (dashed lines) and resin (Supplementary Information, Fig. S2). Nonetheless, both samples showed almost superimposable spectra of their regions attributable to the organic resin, supporting the chemical homology of the resin among the five ES dusts.

### ES dust particles are coated with resin

Using Raman spectroscopy, we explored the extent to which resin coated the different mineral phases of each ES dust (Fig. 2). In High-SiO$_2$ ES1 dust, the resin coated quartz and cristobalite to a low extent but covered half of the rutile and entirely the glassy carbon particles. Several pure resin particles were detected. In Low-SiO$_2$ ES2, the resin coated half of the quartz and all the rutile particles. A few particles of pure resin were detected. In Low-SiO$_2$ ES3 dust, all mineral particles were partially covered with resin, with albite being more extensively coated. In the case of No-SiO$_2$ ES samples, resin coated all (ES4) or the majority (ES5) of gibbsite and GC particles. As expected, no resin was observed in NS. While these results clearly evidenced that resin coated most of the mineral particles in the dust generated by mechanical processing, they did not identify any specific phase that was preferentially coated by the resin.

### Surface charge

The net surface charge, assessed as zeta ($\zeta$) potential by Electrophoretic Light Scattering (ELS), of all ES dusts and NS was markedly negative, with differences among groups of samples (Fig. 3). In 10 mM phosphate buffered saline (PBS) (Fig. 3A), where the pH was 7.4 (physiological) and ionic concentration was isotonic, the samples containing crystalline SiO$_2$ (both high and low) showed slightly more negative surfaces than the No-SiO$_2$ ES dusts and tended towards the highly negative surface of a pure reference quartz (Min-U-Sil 5), which has been analyzed for comparison. This trend was confirmed and enhanced in diluted 1 mM PBS (pH 7.4) (Fig. 3B), where the lower ionic strength caused a higher polarization of the Stern layer surrounding the particles, which in turn enhanced the differences among the dusts. This suggests that the different surface chemistry resulting from the composition and mechanical processing of the High- and Low-SiO$_2$ ES samples with respect to No-SiO$_2$ ES samples played a role on the surface charge of the dusts. Notably, the NS showed $\zeta$ potential values less negative than the reference quartz, despite the absence of the resin. Contaminants, in particular carbon, may reduce the net negative surface charge of pure quartz[37].
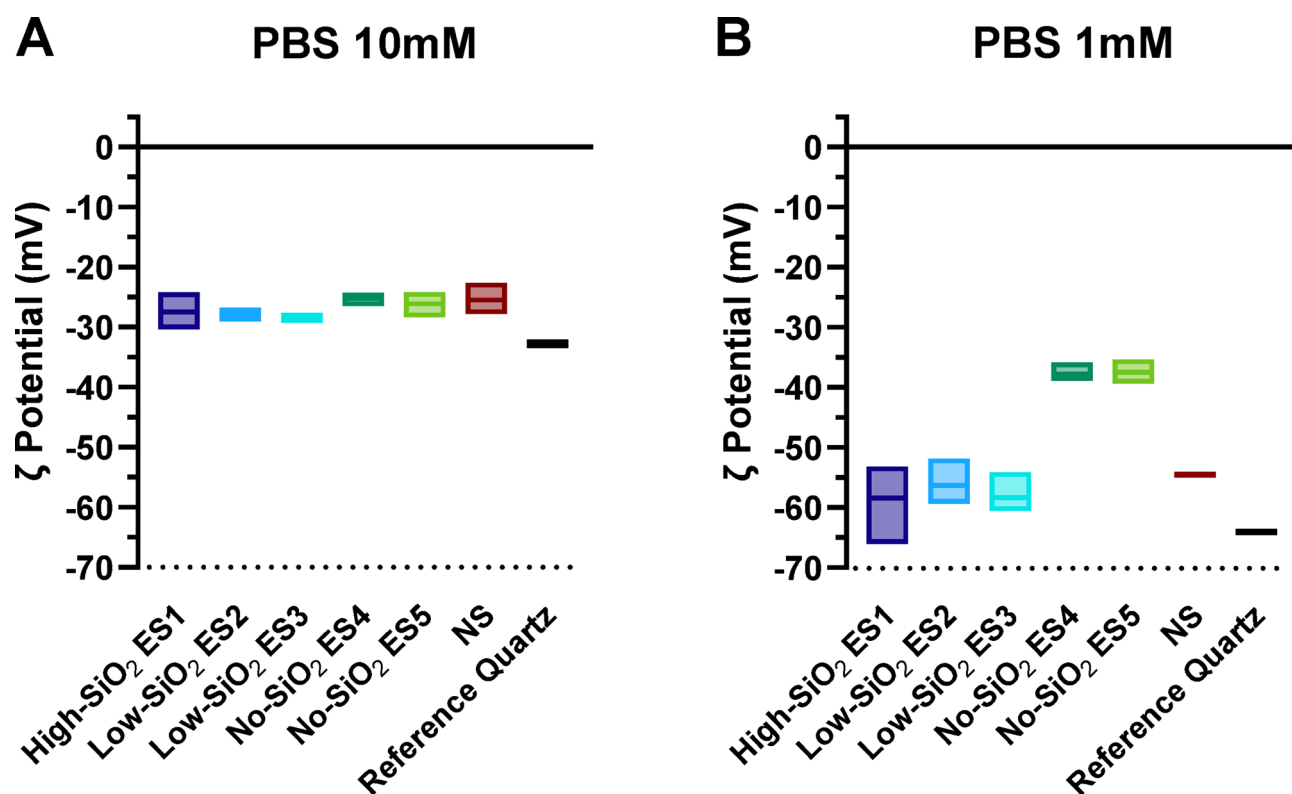


**Fig. 3**. Bar plot of the $\zeta$ potential (mV) of engineered stone (ES1-5), natural stone (NS), and reference quartz (Min-U-Sil 5) particles assessed in PBS at a concentration of **A** 10 mM and **B** 1 mM. Each bar represents the median, min and max values of three independent measurements.
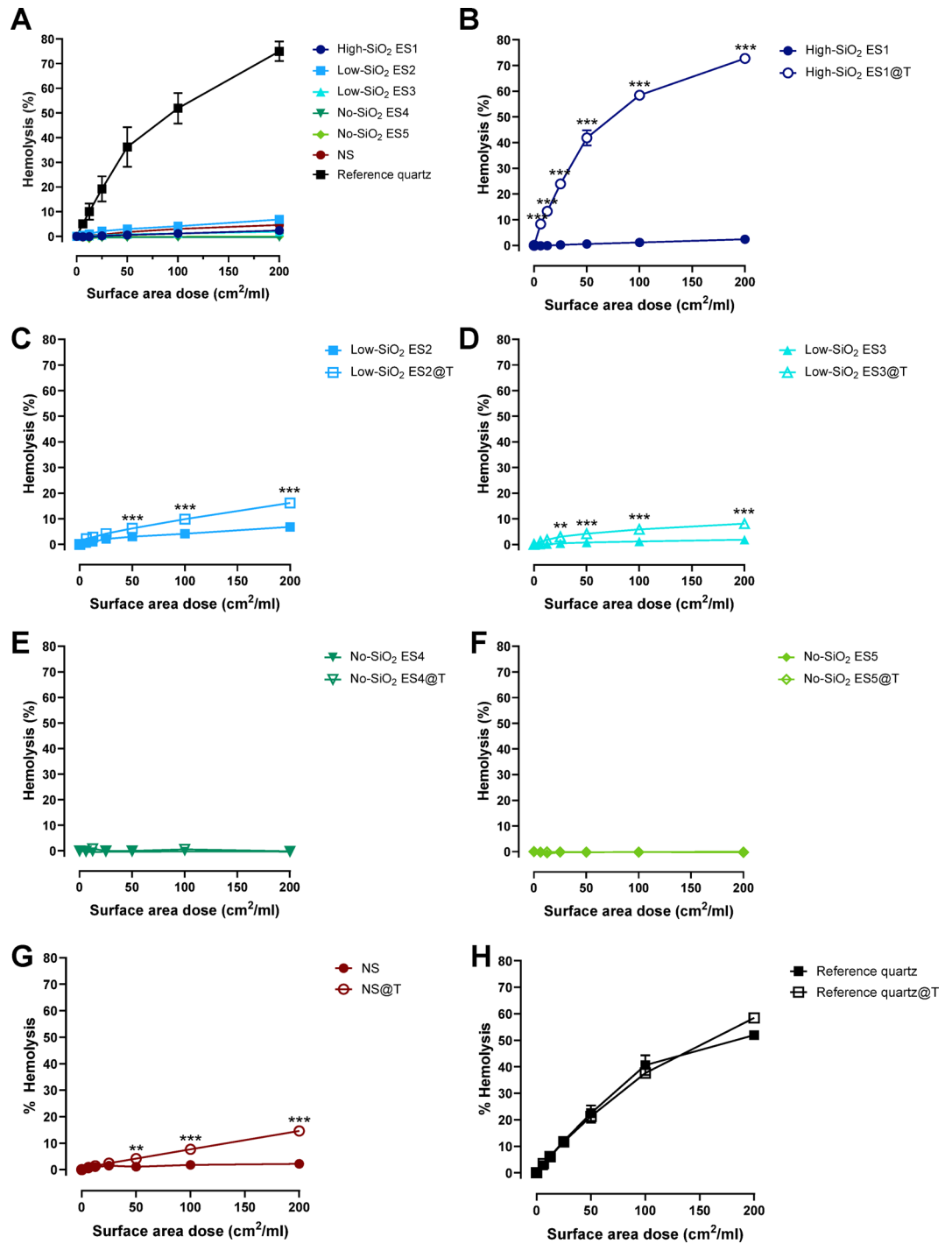
**Fig. 4**. Membranolytic activity (percent hemolysis) of **A** pristine engineered stone (ES1-5), natural stone (NS), and positive reference quartz (Min-U-Sil 5) dusts and **B-H** the same samples after thermal treatment. Increasing surface area doses (0, 6.25, 12.5, 25, 50, 100, and 200 cm$^2$/ml) of ES, NS, and reference quartz dusts were incubated for 30 min with purified sheep RBCs. Values reflect the fraction of the total released hemoglobin content and are reported as mean ± standard error of the mean of at least three independent experiments. Two-way ANOVA and Šidák correction were applied to compare pristine vs. treated dust.

## Membranolysis

The membranolytic activity, which was assessed as the dust capacity to lyse sheep RBCs (i.e., hemolysis), for all ES and NS dust samples is presented in Fig. 4A. The relatively pure quartz (Min-U-Sil 5) was used as a positive reference particle because of its well-established membranolytic and toxic effects[38,39]. All the ES and NS samples showed a negligible or very low membranolytic activity, as compared to the positive reference quartz Min-U-Sil 5 (Fig. 4A). Except for ES2 and NS at the highest dose, all the other samples were below the 2%, which

is considered hemocompatible[40]. There was no correlation between membranolysis and the crystalline $SiO_2$ content of samples. Notably, the membranolytic activity of NS, which was mainly composed by quartz and did not contain resin, was very low compared to the reference quartz Min-U-Sil 5.

Based on TGA analysis, a thermal treatment was applied to remove the polymeric resin that coated ES dust and restore bare mineral surface. In the case of high-$SiO_2$ ES, this treatment has been shown to remove the resin and restore the membranolytic activity of quartz[41]. As expected, the membranolytic activity of High-$SiO_2$ ES1 was drastically increased with respect to the pristine material after heating at 500 °C (Fig. 4B). For Low-$SiO_2$ samples the membranolytic activity increased (Fig. 4C-D), but to a lower extent than High-$SiO_2$ ES1. ES4 and ES5 showed no change (Fig. 4E-F). Interestingly, the thermally treated NS dust showed a significant increase in membranolytic activity (Fig. 4G), although its activity was much lower than samples of comparably high crystalline $SiO_2$ content, e.g. High-$SiO_2$ ES1 (>75% crystalline silica dust). No significant difference was observed between the pristine reference quartz and the heated counterpart (Fig. 4H).

## Discussion

Traditionally, ES contains high levels of crystalline $SiO_2$ mixed with pigments and polymeric resin[1,42]. However, recent developments in ES formulations show lower levels of crystalline $SiO_2$ in the bulk slab, which would likely generate less RCS during mechanical processing of the slab, thus reducing exposures and preventing disease. This change in technology followed strong advocacy from physicians, industry professionals, workers' union groups, and researchers amongst others to raise the alarm about emerging trends of silicosis cases among ES workers worldwide[9,43,44]. Some countries like Australia have imposed a full ban on the use, supply and manufacture of crystalline $SiO_2$-containing ES (>1 wt%) in response to this global crisis[17,45]. To this effect, other parts of the world are now considering a phased-approach to a ban on ES products, e.g., it has been suggested that there be an initial ban in Europe on ES products containing >30% crystalline $SiO_2$, followed by a ban on those of >5% crystalline $SiO_2$ after 5 years[46]. Similarly, experts from the Centre for Occupational and Environmental Health in California recommended a ban on crystalline $SiO_2$-containing ES above a specified threshold, although not yet specified[47]. However, whether recommendations called a full or a partial ban on ES, questions remained about the inadvertent risks that exposure to new ingredients from low- to no-crystalline $SiO_2$ stone benchtop alternatives might pose to workers[47,48]. This research addressed some of these concerns by offering preliminary insights into the material science and surface reactivity towards cellular membranes of dust generated by processing new-generation low- to no-crystalline $SiO_2$ ES products.

Five ES samples and 1 NS sample with variable physico-chemical compositions were compared. When actively processed, High-$SiO_2$ ES1 generated high levels of crystalline $SiO_2$ dust, in the form of quartz (53%) and cristobalite (21%), thus supporting the variable origin of raw materials that are used in the production of ES (Table 2). In comparison, the two Low-$SiO_2$ ES samples generated much lower crystalline $SiO_2$ (<20 and <10 wt%, respectively), in line with their declared composition in the safety data sheets. Minerals in the dusts from Low-$SiO_2$ samples comprised predominantly feldspar (albite), some mica (muscovite), and a large fraction of an amorphous vitreous phase. Rutile, a frequently used white pigment, was found in both High and Low-$SiO_2$ ES dusts. Glassy carbon was also detected in all stone dusts, likely due to its natural presence in many types of rocks (raw materials)[49]. No crystalline silica was analytically detected in the No-$SiO_2$ ES dust samples as they were almost entirely made of aluminium hydroxide (gibbsite) mineral particles (Table 2). Feldspar, mica, and gibbsite are generally considered less toxic than RCS. However, particle inhalation of bauxite (a mixture of aluminum hydroxide minerals, the most abundant of which is gibbsite) may cause the Shaver's disease, a rare occupational lung disease characterized by the development of lung fibrosis, leading to respiratory issues[50]. Prolonged exposure to mica dust has been associated with pneumoconiosis, specifically micaceous pneumoconiosis, a form of interstitial lung disease[51]. In the case of feldspar, the primary health concern is related to the presence of crystalline silica, frequently present as an impurity in feldspar-containing materials. However, recent work by Grytting and colleagues[52] has highlighted the intrinsic bioactivity of specific feldspar minerals, including albite. In their in vitro study, both albite and muscovite demonstrated a high capacity to elicit significant inflammatory and cytotoxic responses, suggesting that certain feldspars may contribute to adverse health effects independently of silica contamination. Nevertheless, due to the high complexity and compositional heterogeneity of the ES samples – including impurities, poorly identifiable amorphous phases, and organic matter – it is essential to evaluate ES dust as a whole when assessing its toxicological potential. As a result, attributing toxicity to a single mineral phase is challenging, underscoring the need for investigation of the dust mixtures. Apart from their mineralogy, other differences in the physico-chemical properties of ES (Low- and No-$SiO_2$) and NS were observed, which are important parameters to assess in toxicity studies as they determine adhesion of particles to cells, and in turn influence their bioavailability and toxic potential[53,54]. Engineered stone samples exhibited a larger population of fine particles, with a MMD ($d$(0.5)) range of 10.2–11.6 μm compared to NS dusts, which exhibited monomodal particle size distribution with MMD of 13.3 μm (Table 1, Fig. S1). Morphology results of High-$SiO_2$ ES1 dust showed particles with sharp edges, conchoidal fractures and irregular surfaces, typical of quartz surfaces obtained by fracturing[31] while aluminium hydroxide (gibbsite) particles in the No-$SiO_2$ ES samples exhibited relatively smooth edges (Fig. 1A). The negative surface charge, measured by the zeta (ζ) potential, observed in crystalline $SiO_2$-containing ES samples and NS was consistent with their mineralogy, as pure or contaminated quartz and (alumino)silicate particles exhibit a net negative surface charge across a wide pH range (ca. 1–8) due to dissociation of silanols or aluminols[55,56]. The difference in ζ potential values between $SiO_2$-containing and $SiO_2$-free dusts may be ascribed to their different mineralogy or coating of the polymeric resin. While all the ES dusts may share the same type of PS-PMMA resin, the No-$SiO_2$ ES samples primarily consisted of aluminium hydroxide (gibbsite), which is reported in the literature as an amphoteric species[57,58]. In those studies, gibbsite showed positive ζ potential values when the pH was below 10. Here, the ζ potential at pH 7.4 of high-gibbsite samples (ES4 and ES5) exhibited negative values. This could be attributed to

the presence of the resin that coated most of ES4 and ES5 particles (Fig. 2). A similar result has been observed in literature for gibbsite modified with polyacrylamide[59]. Moreover, we cannot exclude that the preparation method, which differed between the $SiO_2$-containing (cutting) and No- $SiO_2$ ES samples (milling), may have indirectly influenced the surface charge by altering the surface chemistry, for example through changes in the density or distribution of surface chemical groups.

Resin coating of ES dusts was demonstrated for the first time, using Raman spectroscopy (Fig. 2). Our results suggested that resin coated mineral and amorphous phases of fractured ES dust particles indifferently. This suggests that in real-world exposure scenarios, workers could be inhaling resin-coated dust particles when processing low- to no-$SiO_2$ composite ES samples, the health implications of which are still under debate.

In this study, the coating of mineral phases with resin had a blunting effect against membranolytic activity, as highlighted in Fig. 4A, where all ES dusts exhibited a negligible activity compared to the positive reference quartz. Indeed, by coating the particle surface, resin may mask surface-active groups responsible for the membranolytic activity of quartz and cristobalite – the 'nearly-free silanols' (NFS). The NFS have been previously linked to pro-inflammatory and pro-fibrotic mechanisms causing $SiO_2$-related inflammatory response in the lungs, leading to cellular toxicity and disease[60]. It was interesting to observe that, even though the resin coating of $SiO_2$ (quartz and cristobalite) in High-$SiO_2$ ES1 was low (Fig. 2), it was enough to fully blunt the membranolytic activity of the silica particles (Fig. 4B). This suggests that only some preferential sites on the silica particles could interact with the resin, which were enough to suppress the membranolytic activity of $SiO_2$. We may speculate that these preferential sites could be the NFS as, for a membranolytic quartz, their relative abundance represent only ca. 5% of the total silanols[61].

Notably, despite containing > 80% crystalline $SiO_2$ and clearly no polymeric resin, NS dust induced very low membranolytic activity (ca. 2% at the highest dose tested, Fig. 4A), when untreated. The underlying reasons for this absence of effect compared to other membranolytic natural quartz dusts[38,62] is unclear, possibly because of the mineral origin and surface chemistry. Indeed, quartz in ES stones is generally included as a ground dust, whereas NS is cut directly from rocks to the required slab size, without milling. Since milling is known to enhance the surface reactivity of quartz[29,63]it is possible that the different processing methods of the raw materials influenced the final reactivity of the resulting dusts. Moreover, previous literature has pointed to the occurrence of carbonaceous material such as carbon soot on quartz, that may reduce surface reactivity[37]. Further mechanistic studies integrating surface chemistry properties and cellular uptake is needed to explore why NS particles of high crystalline silica content showed negligible membranolytic activity.

A thermal treatment (500–550 °C) was performed on ES samples to fully remove the resin and expose bare particle surfaces. This treatment was not expected to alter crystalline mineral phases of High and Low-$SiO_2$ ES samples, as confirmed by XRD analysis of the Low-$SiO_2$ ES3 sample (Fig. S3). Thermally treating the $SiO_2$-containing ES samples increased their reactivity, underlining the relevance of $SiO_2$ in inducing membrane damage even when found in a complex matrix. In decreasing order of activity for heated ES samples were High-$SiO_2$ ES1 > Low-$SiO_2$ ES2 > Low-$SiO_2$ ES3 > No-$SiO_2$ ES4 = No-$SiO_2$ ES5. At the highest dose level, Low-$SiO_2$ ES2, which contained ca. 3 times more $SiO_2$ than Low-$SiO_2$ ES3 (Table 2), induced twice as much hemolytic activity (Fig. 4C, D). This dose-response relationship between crystalline $SiO_2$ content and membranolytic activity again suggested the presence of the NFS population and its role in inducing membranolysis. Low-$SiO_2$ ES3 also contained feldspar and mica as fillers, which exhibited a negligible membranolytic activity in previous studies[52]. The low but measurable hemolytic activity observed for low-$SiO_2$ samples could also be ascribed to their amorphous vitreous phase content, which was higher in Low-$SiO_2$ ES2 and paralleled its more pronounced hemolytic activity. However, the composition of this vitreous phase and its role in membranolysis is still unclear. Some studies have shown that vitreous silica and (aluminium) silicates exhibit hemolytic activity[27,56,64]suggesting a potential contribution of these phases to membranolysis. In comparison, No-$SiO_2$ ES dusts were not hemolytic (Fig. 4E-F), in line with previous findings that gibbsite, the main mineral phase in No-$SiO_2$ ES samples, is not hemolytic[65] (Fig. 4E-F). Heating No-$SiO_2$ ES4 at 550 °C led to the formation of amorphous alumina ($\chi$-$Al_2O_3$) as assessed by XRD analysis (Fig. S3), consistent with known thermal decomposition behaviour of gibbsite[66]. Alumina, like gibbsite, was also non-hemolytic as previously reported[26]. The thermal treatment of NS dust increased its membranolytic activity, albeit being a resin-free dust. This increase in activity is likely due to an increase in the NFS content, as consequence of the partial dehydration of silanols at the surface of quartzite, as previously observed for a pure quartz[61].

Some limitations in the design of this study should be considered when interpreting the results. Although the slabs were carefully selected to represent a range of $SiO_2$ content, only five slabs were investigated, and a larger sample size is necessary to draw broader conclusions about the potential hazards of emerging low- to no-$SiO_2$ stone composites during mechanical processing.

Due to limited material availability, two slabs (No-$SiO_2$ ES4 and ES5) were processed by milling rather than by active cutting with an angle grinder, which was used for the other samples. While milling can replicate the high-energy particle generation typical of cutting operations, this methodological difference may have affected the physico-chemical characteristics and surface reactivity of the resulting dust from No-$SiO_2$ ES4 and ES5, including particle size distribution and the resin coating pattern on mineral phases. Although the milling protocol was optimized to generate particles within a size range comparable to that of dust from actively cut ES, as evidenced by similar $d(0.5)$ values across the samples, No-$SiO_2$ ES4 and ES5 dusts exhibited a larger fraction of fine particles. This difference could be attributed either to the milling process itself or to intrinsic material composition, both of which may influence the physico-chemical properties of the dust, including the pattern of resin coating on mineral phases.

These variations in particle size distribution may affect SSA and the membranolytic activity of the ES dusts[67]. In fact, No-$SiO_2$ ES4 and ES5, which had more fine particles, also showed higher SSA values. Increased SSA of quartz particles is often associated with greater membranolytic activity than larger ones[68,69]; however, this trend

was not supported by the current findings. The High- $SiO_2$ ES1 sample, which had the coarsest particle size distribution, demonstrated the highest hemolytic activity after resin removal, reaching levels comparable to the respirable Min-U-Sil-5. As heating does not affect particle size or SSA, this suggests that surface chemistry and particle composition, rather than particle size alone, play a dominant role in driving the hemolytic potential of ES dusts. It should be noted that, in the hemolysis assay, particle dose was normalized to the particle-specific surface area to account for surface exposure and, to some extent, differences in particle size.

It is important to note that 90% of the particles (%volume) explored in this study had particle size larger than the respirable fraction (4.0 μm aerodynamic diameter)[70]. As such, the results presented did not represent realistic exposure scenarios but rather showed an evaluation of the physico-chemical characteristics and membranolytic effect of as-cut and freshly-fractured dust particles. Future research should prioritize the assessment of health risks associated with respirable dust fractions, which are more relevant in occupational exposure settings. Moreover, while the hemolysis assay provided an initial assessment of particle surface reactivity and cellular toxicity[71] its relevance for occupational health outcomes requires further validation using well-established high throughput in vitro lung cell assays or in vivo experiments. This is especially important because hemolysis has previously been shown to reflect the inflammatory activity of $SiO_2$ dust in occupational settings[27,62] and as emerging ES alternatives contain lower $SiO_2$ levels, it becomes increasingly important to determine whether hemolysis remains a reliable toxicity model.

In conclusion, the study demonstrated that dusts generated by mechanically processing low- to no-$SiO_2$ ES were heterogenous in chemical composition, with many particles fully or partially coated by polymeric resin. When the resin was thermally removed, Low-$SiO_2$ ES dusts caused less, though still significant, damage to the cell membrane compared to High-$SiO_2$ ES particles, indicating a primary crystalline $SiO_2$-related membranolytic effect. As the $SiO_2$ content in ES dusts lowered to nil, other mineral phases such as silicates, aluminium hydroxide, and a vitreous phase were identified. The toxicological significance of these new phases remain unclear and require thorough physico-chemical characterization and toxicity testing for a more complete assessment of hazards in the stone benchtop workplace. Comprehensive assessment of airborne dusts from emerging ES benchtop alternatives such as low-$SiO_2$ stone products, including porcelain, ceramics, sintered stone, and natural stone is urgently needed to inform occupational health and safety recommendations and regulations aimed at preventing dust-related diseases.

## Materials and methods
### Stone samples
Five ES samples of varying $SiO_2$ levels (from 90 to 0 wt%) were included in this study. In decreasing order of their reported $SiO_2$ contents, the samples were High-$SiO_2$ ES1 (51–90%), Low-$SiO_2$ ES2 (<28%), Low-$SiO_2$ ES3 (<10%), No-$SiO_2$ ES4 (0%) and No-$SiO_2$ ES5 (0%). One natural stone (NS) (>90%) was also included for comparison. All stone samples were sourced as a final product from commercial stone suppliers in Australia.

### Dust generation
Engineered stone samples ES1-3 and the NS were actively cut using an angle grinder (Metabo 720 W), fitted with a 105 mm diamond blade and operating at ~10,000 rpm (Digital Tachometer QM1448, New England Instrument Co., NEIC), in a custom-built test chamber at the University of Adelaide, as described in Ramkissoon et al. (2022)[28]. After mechanical grinding, the dust that settled in the test chamber was collected and subjected to physico-chemical characterization. In comparison, due to insufficient slab dimension for mechanical grinding (thereby risking operator's safety), ES4 and ES5 were not actively cut; instead, slabs were ground to a coarse powder in agate jars on a planetary mill (Vibratory Micro Mill PULVERISETTE 0, FRITSCH GmbH, NSW, Australia) at 70 RPM for 45 min; 0.5 g of these samples were further ground at 27 Hz for 60 min in agate jars, with two agate balls of 6 mm diameter per jar, on a mixer mill (MM 200 Mixer Mill, RETSCH GmbH, Haan, Germany). All collected dust samples were stored in cool, dry conditions prior to analysis.

The commercial quartz Min-U-Sil 5 (US Silica Company, Berkeley Springs, WV, USA) was used as reference particle because it has been extensively characterized in previous studies and has well-known membranolytic and toxic effects[38,61,72]. It is a relatively pure quartz (98.8 wt% $SiO_2$ and 1.2 wt% $Al_2O_3$), characterized by a SSA of 5.0 $m^2$/g and average particle diameter of $1.9 \pm 0.9$ μm[38].

### Physico-chemical characterization
*Particle size*
Particle size was determined by laser diffractometry on a Mastersizer 2000 (Malvern Instruments, UK). Dry stone powder samples were dispersed in water until an obscuration level of ~15%. Refraction indices ranged from 1.4 to 1.6, depending on the sample mineralogy.

*Morphology and elemental composition*
The morphology and chemical analysis of the dust particles was examined by SEM-EDS with a Tescan VEGA 4 microscope equipped with an Oxford AZTEC Ultim Max EDS detector. Secondary electron images were acquired at various magnifications (from 1,000× up to 25000×) and accelerating voltages, commonly 10–15 kV. Operating conditions for EDS analysis were 15 kV and 100 pA, 105 CPS and 30 s counting time. Relative percent weight (wt%) errors were <1% for major elements and <5% for minor components. Powder samples were first dispersed in ultrapure water (at ~0.5 mg/ml), sonicated for 5 min (40 W; Sonoplus, Bandelin, Berlin, Germany), dropped off on conductive stubs and coated with carbon. Dispersing the particles in water enhanced their distribution and facilitated more uniform deposition on the stub[73].

*Mineral phases*

Quantitative analysis for the $SiO_2$ (i.e. quartz, cristobalite and tridymite) content of stone dust samples was done by XRD, based on the National Institute for Occupational Safety and Health (NIOSH) analytical 7500 thin film filter method. The detection limit for quartz and cristobalite was estimated to be 0.1 wt%. The tridymite detection limit was estimated to be 0.3%. Phase transformation of heated ES dusts was assessed by XRD using a PW3040/60 X'Pert PRO MPD diffractometer (PANalytical) in the spinning configuration. Diffractograms were collected in the 2θ range from 5 to 90°, with a step size of 0.0167°, 0.042 °/s of speed, and CuKα radiation at 45 kV and 40 mA. The diffractograms obtained were analyzed with the PANalytical X'Pert HighScore software.

Further qualitative analysis of the mineral phases of the stone dust samples was undertaken by micro-Raman Spectroscopy. Raman spectra were acquired using a Horiba Jobin Yvon HR800 Raman spectrometer, integrated with an Olympus BX41 confocal microscope. The system utilised a 600 grooves/mm holographic grating monochromator and a high-gain CCD Peltier detector. Excitation was achieved using a 532 nm Nd solid-state laser, and neutral density filters were employed to mitigate thermal effects and prevent sample overheating. Measurements were performed on 50 particles per sample using a 100× objective lens. The experimental setup provided a minimum lateral resolution of approximately 2 μm and a depth (z-axis) resolution of ca. 1 μm. Calibration of the spectrometer was conducted prior to each experimental session using the 520.7 cm⁻¹ Raman band of silicon. Spectra were collected as follows: 3 acquisitions for 20 s in the low and high wavenumber spectral range were averaged and background subtracted with LabSpec* software.

*Specific surface area*

The SSA of stone dusts was measured by the Brunauer, Emmett, and Teller (BET) method based on Kr adsorption at −196 ⁰C, using a 3Flex adsorption analyser (Micromeritics, Norcross, USA). All samples were degassed at 30 ⁰C for 12 h prior to analysis.

*Organic content and characterization*

Degradation of resin in ES samples was assessed by TGA. Approximately 10 mg of ES dust was heated in a $N_2$ atmosphere (flow rate of 50 ml/min) up to 600 °C at the rate of 10 ⁰C/min. Weight loss after sample pyrolysis was determined by an ultra-microbalance (0.1 μg) (Mettler-Toledo, Inc., TGA/DSC 2 STARe System, Columbus, Ohio, USA).

*Surface charge*

ES dusts were dispersed in 0.01 M or 0.001 M phosphate buffered saline (PBS, Sigma Aldrich, USA) (0.6 mg/ml, pH 7.4) and sonicated for 2 min in an ultrasound bath (Falc, Italy), just before testing. Particle surface charge (ζ potential) was measured by Electrophoretic Light Scattering (ELS) using a Zetasizer Nano ZS (Malvern Instruments, UK). Data were obtained by three independent measures, five replicates for each measurement.

## Membranolysis

The method refers to previous studies[38,56] with minor modifications. In short, RBCs were purified from sheep blood in Alsever's solution (Thermo Scientific, Oxoid, UK) by centrifugation at 3,000 ×g for 2 min (Rotina 380R; Hettich, MA) and washing three times with 0.9% NaCl (Eurospital, Italy). RBCs were suspended in 0.01 M PBS (Sigma Aldrich, USA) at the final concentration of 5% by volume. ES dusts were dispersed in 0.01 M PBS and sonicated 2 min in an ultrasound bath (Falc, Italy), just before testing. Serial dilutions of the starting particle dispersions were performed according to the final surface area doses used for experiments. Dispersions were distributed in quadruplicate in a transparent 96-well plate (150 μl/well), and the RBC suspension was then added (75 ml/well). Negative and positive controls consisted of 0.01 M PBS and 0.1% Triton X-100 in PBS, respectively. The plate was incubated on a plate shaker at 37 °C for 30 min, and then centrifuged at 216 g for 5 min. Supernatants were transferred to a new plate (75 ml/well), and the absorbance of the haemoglobin released was determined at 540 nm on a UV/vis spectrophotometer (Ensight, Perkin-Elmer, Waltham, USA) using the software Kaleido 2.0 (Perkin-Elmer).

*Thermal treatment*

To remove the organic material, including the polymeric resin[41] the pristine ES dusts (500 mg) were heated in a muffle furnace (Nabertherm, Germany) at 500 °C (ES1, ES2, and ES3) or 550 °C (ES4 and ES5) for 1 h (ramp up: 10 °C/min). For comparison purposes, samples not containing resin (NS and reference quartz) were also heated at 500 °C. Samples were stored in a cool and dry environment before testing hemolysis.

## Statistics

Statistical parameters, including the number of independent experiments and statistical significance, are reported in the figures and figure legends. Unless otherwise stated, data are presented as mean ± standard error of the mean.

## Data availability

The datasets generated during and/or analysed during the current study are available from the corresponding authors on reasonable request.

# References

1. Kumarasamy, C., Pisaniello, D., Gaskin, S. & Hall, T. What do safety data sheets for artificial stone products tell Us about composition? A comparative analysis with physicochemical data. *Ann. Work Expo Health.* **66**, 937–945 (2022).
2. Mandler, W. K., Qi, C. & Qian, Y. Hazardous dusts from the fabrication of countertop: a review. *Int. Arch. Occup. Environ. Health.* **78**, 118–126. https://doi.org/10.1080/19338244.2022.2105287 (2023).
3. Leso, V., Fontana, L., Romano, R., Gervetti, P. & Iavicoli, I. Artificial stone associated silicosis: A systematic review. *Int. J. Environ. Res. Public. Health.* **16**, 568. https://doi.org/10.3390/ijerph16040568 (2019).
4. Hoy, R. F. et al. Artificial stone-associated silicosis: A rapidly emerging occupational lung disease. *Occup. Environ. Med.* **75**, 3–5. https://doi.org/10.1136/oemed-2017-104428 (2018).
5. Hua, J. T., Rose, C. S. & Redlich, C. A. Engineered stone–associated silicosis—A lethal variant of an ancient disease. *JAMA Intern. Med.* **183**, 908–910. https://doi.org/10.1001/jamainternmed.2023.3260 (2023).
6. Fazio, J. C. et al. Silicosis among immigrant engineered stone (quartz) countertop fabrication workers in California. *JAMA Intern. Med.* **183**, 991–998. https://doi.org/10.1001/jamainternmed.2023.3295 (2023).
7. Kramer, M. R. et al. Artificial stone silicosis [corrected]: disease resurgence among artificial stone workers. *Chest* **142**, 419–424. https://doi.org/10.1378/chest.11-1321 (2012).
8. Hoy, R. F. et al. Prevalence and risk factors for silicosis among a large cohort of stone benchtop industry workers. *Occup. Environ. Med.* **80**, 439–446. https://doi.org/10.1136/oemed-2023-108892 (2023).
9. Hua, J. T. et al. Demographic, exposure and clinical characteristics in a multinational registry of engineered stone workers with silicosis. *Occup. Environ. Med.* **79**, 586–593. https://doi.org/10.1136/oemed-2021-108190 (2022).
10. Pérez-Alonso, A. et al. Outbreak of silicosis in Spanish quartz conglomerate workers. *Int. J. Environ. Res. Public. Health.* **20**, 26–32. https://doi.org/10.1179/2049396713Y.0000000049 (2014).
11. Pérez-Alonso, A., Córdoba-Doña, J. A. & León-Jiménez, A. Silicosis caused by artificial quartz conglomerates: keys to controlling an emerging disease. *Arch. Bronconeumol. (English ed.).* **55**, 394–395. https://doi.org/10.1016/j.arbr.2019.01.002 (2019).
12. Pérez-Alonso, A., González-Domínguez, M. E., Novalbos-Ruiz, J. P., León-Jiménez, A. & Córdoba-Doña, J. A. Artificial stone silicosis: accumulation of errors in the resurgence of an occupational disease: A qualitative study. *Work (Reading Mass).* **70**, 433–442. https://doi.org/10.3233/WOR-213582 (2021).
13. Ronsmans, S., Decoster, L., Keirsbilck, S., Verbeken, E. K. & Nemery, B. Artificial stone-associated silicosis in Belgium. *Occup. Environ. Med.* **76**, 133–134. https://doi.org/10.1136/oemed-2018-105436 (2019).
14. Rose, C. et al. Severe silicosis in engineered stone fabrication workers — California, colorado, texas, and washington, 2017–2019. *MMWR* **68**, 813–818. https://doi.org/10.15585/mmwr.mm6838a1 (2019).
15. Feary, J. et al. Artificial stone silicosis: A UK case series. *Thorax* **79**, 979–981. https://doi.org/10.1136/thorax-2024-221715 (2024).
16. Guarnieri, G. et al. Silicosis in finishing workers in quartz conglomerates processing. *Med. Lav.* **111**, 99–106. https://doi.org/10.23749/mdl.v111i2.9115 (2020).
17. Nogrady, B. Australia bans engineered stone because of silicosis risk. *BMJ* **383**, 2954–2954. https://doi.org/10.1136/bmj.p2954 (2023).
18. Kirby, T. Australia bans engineered stone to prevent silicosis. *Lancet Respir Med.* **12**, e18–e18. https://doi.org/10.1016/S2213-2600(24)00007-9 (2024).
19. Wise, J. Doctors call for ban on cutting artificial stone after reporting first UK cases of silicosis. *BMJ* . **386** (q1755). https://doi.org/10.1136/bmj.q1755 (2024).
20. NIOSH. *About Hierarchy of Controls,* https://www.cdc.gov/niosh/hierarchy-of-controls/about/index.html#print (2024)
21. Ramkissoon, C., Gaskin, S., Song, Y., Pisaniello, D. & Zosky, G. R. From engineered stone slab to silicosis: A synthesis of exposure science and medical evidence. *Int. J. Environ. Res. Public. Health.* **21**, 683. https://doi.org/10.3390/ijerph21060683 (2024).
22. Ramkissoon, C. et al. Understanding the pathogenesis of engineered stone-associated silicosis: the effect of particle chemistry on the lung cell response. *Respirol. (Carlton Vic).* **29**, 217–227. https://doi.org/10.1111/resp.14625 (2024).
23. Rishi, K. et al. Release of crystalline silica nanoparticles during engineered stone fabrication. *ACS Omega.* **9**, 50308–50317. https://doi.org/10.1021/acsomega.4c06437 (2024).
24. Jessop, F., Hamilton, R. F., Rhoderick, J. F., Fletcher, P. & Holian, A. Phagolysosome acidification is required for silica and engineered nanoparticle-induced lysosome membrane permeabilization and resultant NLRP3 inflammasome activity. *Toxicol. Appl. Pharmacol.* **318**, 58–68. https://doi.org/10.1016/j.taap.2017.01.012 (2017).
25. Pavan, C. & Fubini, B. Unveiling the variability of quartz hazard in light of recent toxicological findings. *Chem. Res. Toxicol.* **30**, 469–485. https://doi.org/10.1021/acs.chemrestox.6b00409 (2017).
26. Lu, S. et al. Efficacy of simple short-term *in vitro* assays for predicting the potential of metal oxide nanoparticles to cause pulmonary inflammation. *Environ. Health Perspec.* **117**, 241–247. https://doi.org/10.1289/ehp.11811 (2009).
27. Pavan, C., Rabolli, V., Tomatis, M., Fubini, B. & Lison, D. Why does the hemolytic activity of silica predict its pro-inflammatory activity? *Part. Fibre Toxicol.* **11**, 76–76. https://doi.org/10.1186/s12989-014-0076-y (2014).
28. Ramkissoon, C. et al. Characterisation of dust emissions from machined engineered stones to understand the hazard for accelerated silicosis. *Sci. Rep.* **12**, 4351–4351. https://doi.org/10.1038/s41598-022-08378-8 (2022).
29. Bellomo, C., Lagostina, V., Pavan, C., Paganini, M. C. & Turci, F. Reaction with water vapor defines surface reconstruction and membranolytic activity of quartz milled in different molecular environments. *Small* **20**, e2308369–n. https://doi.org/10.1002/smll.202308369 (2024).
30. Ilić, M. et al. Size and shape particle analysis by applying image analysis and laser diffraction – Inhalable dust in a dental laboratory. *Meas. : J. Int. Meas. Confed.* **66**, 109–117. https://doi.org/10.1016/j.measurement.2015.01.028 (2015).
31. Turci, F. et al. Revisiting the paradigm of silica pathogenicity with synthetic quartz crystals: the role of crystallinity and surface disorder. *Part. Fibre Toxicol.* **13**, 32. https://doi.org/10.1186/s12989-016-0136-6 (2016).
32. Bellomo, C. et al. Top-down Preparation of Nanoquartz for toxicological investigations. *Int. J. Mol. Sci.* **23**, 15425. https://doi.org/10.3390/ijms232315425 (2022).
33. Friedmann, T. A., Siegal, M. P., Tallant, D. R., Simpson, R. L. & Donminguez, F. Residual stress and Raman spectra of laser deposited highly tetrahedral-coordinated amorphous carbon films. *MRS Online Proc. Libr.* **349**, 501–506. https://doi.org/10.1557/PROC-349-501 (1994).
34. Whitney, D. L. & Evans, B. W. Abbreviations for names of rock-forming minerals. *Am. Min.* **95**, 185–187. https://doi.org/10.2138/am.2010.3371 (2010).
35. Briley, E., Huestis, P., Zhang, X., Rosso, K. M. & LaVerne, J. A. Radiolysis of thermally dehydrated gibbsite. *Mater. Chem. Phys.* **271**, 124885. https://doi.org/10.1016/j.matchemphys.2021.124885 (2021).
36. Thomas, K. J., Sheeba, M., Nampoori, V. P. N., Vallabhan, C. P. G. & Radhakrishnan, P. Raman spectra of polymethyl methacrylate optical fibres excited by a 532 Nm diode pumped solid state laser. *J. Opt. -Pure Appl. Op.* **10**, 055303. https://doi.org/10.1088/1464-4258/10/5/055303 (2008).
37. Ghiazza, M. et al. Carbon in intimate contact with quartz reduces the biological activity of crystalline silica dusts. *Chem. Res. Toxicol.* **26**, 46–54. https://doi.org/10.1021/tx300299v (2013).
38. Pavan, C. et al. Nearly free Silanols drive the interaction of crystalline silica polymorphs with membranes: implications for mineral toxicity. *Front. Chem.* **10**, 1092221–1092221. https://doi.org/10.3389/fchem.2022.1092221 (2023).
39. IARC. *Arsenic, Metals, Fibres and Dusts* (International Agency for Research on Cancer (IARC), 2012).

40. Tiwari, K. et al. Surface modification of Ti40Cu40Zr11Fe3Sn3Ag3 amorphous alloy for enhanced biocompatibility in implant applications. *J. Mater. Res. Technol.* **30**, 2333–2346. https://doi.org/10.1016/j.jmrt.2024.03.225 (2024).
41. Pavan, C. et al. (eds) 's Highlight: Abrasion of Artificial Stones as a New Cause of an Ancient Disease. Physicochemical Features and Cellular Responses. *Toxicol. Sci.* 153, 4–17 https://doi.org/10.1093/toxsci/kfw101 (2016).
42. Agrizzi, C. P. et al. Comparison between synthetic and biodegradable polymer matrices on the development of quartzite waste-based artificial stone. *Sustainability* **14**, 6388. https://doi.org/10.3390/su14116388 (2022).
43. Hoy, R. F. et al. Current global perspectives on silicosis—Convergence of old and newly emergent hazards. *Respirol. (Carlton Vic).* **27**, 387–398. https://doi.org/10.1111/resp.14242 (2022).
44. Hoy, R. F. et al. Identification of early-stage silicosis through health screening of stone benchtop industry workers in victoria, Australia. *Occup. Environ. Med.* **78**, 296–302. https://doi.org/10.1136/oemed-2020-106897 (2021).
45. Glass, D. C. & Hoy, R. F. The leadup to the artificial stone ban in Australia. *Ann. Work Expo Health.* https://doi.org/10.1093/annweh/wxae085 (2024).
46. Kromhout, H., van Tongeren, M. & Cherrie, J. W. Should engineered stone products be banned? *Occup. Environ. Med.* oemed-2024-109708 https://doi.org/10.1136/oemed-2024-109708 (2024).
47. Jones, R. M. & Batteate, C. *Preventing Silicosis: Meeting Report and Recommendations. (Center for Occupational and Environmental Health, Fielding School of Public Health* (University of California, Los Angeles, 2024).
48. Carey, R. & Ramkissoon, C. in *The Conversation* (2024).
49. Robinson, G. R., Hammarstrom, J. M. & Olson, D. W. in *Critical mineral resources of the United States; economic and environmental geology and prospects for future supply* (eds K. J. Schulz, D. C. Bradley, R. R. Seal, & J. H. DeYoung)U. S. Dept. of the Interior, U. S. Geological Survey, (2017).
50. Jones, T. & BéruBé, K. A. in *In Particle Toxicology*. 13–34 (eds Donaldson, K. & Borm, P.) (CRC Press Taylor & Francis Group, 2006).
51. Skulberg, K. R., Gylseth, B., Skaug, V. & Hanoa, R. Mica pneumoconiosis-A literature review. *Scand. J. Work Environ. Health.* **11**, 65–74. https://doi.org/10.5271/sjweh.2250 (1985).
52. Grytting, V. S. et al. The importance of mineralogical composition for the cytotoxic and pro-inflammatory effects of mineral dust. *Part. Fibre Toxicol.* **19**, 1–46. https://doi.org/10.1186/s12989-022-00486-7 (2022).
53. Silva, T. et al. Particle size, surface charge and concentration dependent ecotoxicity of three organo-coated silver nanoparticles: comparison between general linear model-predicted and observed toxicity. *Sci. Total Environ.* **468–469**, 968–976. https://doi.org/10.1016/j.scitotenv.2013.09.006 (2014).
54. Vattanasit, U., Kongpran, J. & Ikeda, A. Airborne microplastics: A narrative review of potential effects on the human respiratory system. *Sci. Total Environ.* **904**, 166745–166745. https://doi.org/10.1016/j.scitotenv.2023.166745 (2023).
55. Pavan, C. et al. Z potential evidences Silanol heterogeneity induced by metal contaminants at the quartz surface: implications in membrane damage. *Colloids Surf. B Biointerfaces.* **157**, 449–455. https://doi.org/10.1016/j.colsurfb.2017.06.012 (2017).
56. Cananà, S. et al. Interaction of layered silicates with biomembranes: Ion exchangers and non-exchangers. *Adv. Mater. Interfaces* 9, https://doi.org/10.1002/admi.202201347 (2022).
57. Adekola, F. et al. Characterization of acid–base properties of two gibbsite samples in the context of literature results. *J. Colloid Interface Sci.* **354**, 306–317. https://doi.org/10.1016/j.jcis.2010.10.014 (2011).
58. Zhang, Z. et al. Co-transport of U(VI) and bentonite colloids; influence of colloidal gibbsite. *Appl. Clay Sci.* **205**, 106033. https://doi.org/10.1016/j.clay.2021.106033 (2021).
59. Szewczuk-Karpisz, K. et al. Electrical double layer at the gibbsite/anionic polyacrylamide/supporting electrolyte interface – Adsorption, spectroscopy and electrokinetic studies. *J. Mol. Liq*. **261**, 439–445. https://doi.org/10.1016/j.molliq.2018.04.030 (2018).
60. Pavan, C. et al. Short- and long-term pathologic responses to quartz are induced by nearly free Silanols formed during crystal fracturing. *Part. Fibre Toxicol.* **21**, 52–13. https://doi.org/10.1186/s12989-024-00611-8 (2024).
61. Pavan, C. et al. Nearly free surface Silanols are the critical molecular moieties that initiate the toxicity of silica particles. *PNAS* **117**, 27836. https://doi.org/10.1073/pnas.2008006117 (2020).
62. Clouter, A., Brown, D., Höhr, D., Borm, P. & Donaldson, K. Inflammatory effects of respirable quartz collected in workplaces versus standard DQ12 quartz: particle surface correlates. *Toxicol. Sci.* **63**, 90–98. https://doi.org/10.1093/toxsci/63.1.90 (2001).
63. Vallyathan, V. et al. Freshly fractured quartz inhalation leads to enhanced lung injury and inflammation. Potential role of free radicals. *Am. J. Respir Crit. Care Med.* **152**, 1003–1009. https://doi.org/10.1164/ajrccm.152.3.7663775 (1995).
64. Hunt, J., Pooley, F. D. & Richards, R. J. Biological reactivity of calcium silicate composites— in vitro studies. *Environ. Res.* **26**, 51–68. https://doi.org/10.1016/0013-9351(81)90183-3 (1981).
65. Oscarson, D. W., Van Scoyoc, G. E. & Ahlrichs, J. L. Lysis of erythrocytes by silicate minerals. *Clays Clay Min.* **34**, 74–80. https://doi.org/10.1346/CCMN.1986.0340109 (1986).
66. Malki, A. et al. Calcination products of gibbsite studied by X-ray diffraction, XPS and solid-state NMR. *J. Solid State Chem.* **215**, 8–15. https://doi.org/10.1016/j.jssc.2014.03.019 (2014).
67. Pavan, C. et al. In search of the chemical basis of the hemolytic potential of silicas. *Chem. Res. Toxicol.* **26**, 1188–1198. https://doi.org/10.1021/tx400105f (2013).
68. Wiessner, J. H., Mandel, N. S., Sohnle, P. G. & Mandel, G. S. Effect of particle size on quartz-induced hemolysis and on lung inflammation and fibrosis. *Exp. Lung Res.* **15**, 801–812. https://doi.org/10.3109/01902148909069627 (1989).
69. Nolan, R. P., Langer, A. M. & Foster, F. W. in *In vitro effects of mineral dusts* Vol. 3 *NATO ASI Series* (eds J. Bignon & E. G. Beck) 39–50Springer Berlin, Heidelberg, (1985).
70. Brown, J. S., Gordon, T., Price, O. & Asgharian, B. Thoracic and respirable particle definitions for human health risk assessment. *Part. Fibre Toxicol.* **10**, 12–12. https://doi.org/10.1186/1743-8977-10-12 (2013).
71. Greco, I. et al. Correlation between hemolytic activity, cytotoxicity and systemic in vivo toxicity of synthetic antimicrobial peptides. *Sci. Rep.* **10**, 13206. https://doi.org/10.1038/s41598-020-69995-9 (2020).
72. IARC. in Arsenic, Metals, Fibres and Dusts Vol. 100 C (ed IARC Working Group on the Evaluation of Carcinogenic Risks to Humans). International Agency for Research on Cancer, (2012).
73. 20720:2018 *I. Microbeam Analysis — Methods of Specimen Preparation for Analysis of General Powders Using WDS and EDS* (International Standards Organization, 2018).

## Acknowledgements

## Author contributions

C.R. and C.P. were involved in the conceptualisation and design of the study, data analysis and interpretation, drafted and finalised the manuscript. J.R.P. was involved in the design of the study, data analysis and interpre-

## Declarations

## Competing interests
The authors declare no competing interests.

## Additional information
**Supplementary Information** The online version contains supplementary material available at https://doi.org/10.1038/s41598-025-10460-w.

**Correspondence** and requests for materials should be addressed to C.R. or C.P.

**Reprints and permissions information** is available at www.nature.com/reprints.

**Publisher's note** Springer Nature remains neutral with regard to jurisdictional claims in published maps and institutional affiliations.